International Communications in Heat and Mass Transfer 116 (2020) 104639

Contents lists available at ScienceDirect

International Communications in Heat and Mass Transfer

journal homepage: www.elsevier.com/locate/ichmt

On the unsteady forced convection in porous media subject to inlet flow disturbances-A pore-scale analysis

Rabeeah Habib[a], Bijan Yadollahi[a], Nader Karimi[a,*], Mohammad Hossein Doranegard[b]

[a] James Watt School of Engineering, University of Glasgow, Glasgow G12 8QQ, United Kingdom
[b] Department of Civil and Environmental Engineering, School of Mining and Petroleum Engineering, University of Alberta, Edmonton, Alberta T6G 1H9, Canada

ARTICLE INFO

Keywords:
Unsteady forced convection
Porous media
Frequency response
Pore-scale analysis
Transfer function
Nonlinear dynamics

ABSTRACT

Heat convection response of a porous medium to the harmonic disturbances in the inlet flow is investigated in a configuration consisting of several obstacles. Navier Stokes and energy equations are solved computationally and the average Nusselt number around the obstacles is favourably compared against the existing empirical data. The Nusselt number fluctuations are then examined, revealing that the dynamical relations between the inlet flow fluctuations as the input and those of Nusselt number as the output, can be nonlinear. The extent of encountered nonlinearity is determined quantitatively through introduction of a measure of nonlinearity. It is shown that increases in the pore-scale Reynolds number can strengthen the nonlinearity. However, this is not a global trend and further increases in Reynolds number may push the system dynamics back to linear. Application of the concept of transfer function to the identified linear cases reveals that the frequency response of the Nusselt number closely resembles a classical low-pass filter. Further, through a statistical analysis, it is shown that thermal response of the porous medium is strongly dominated by those of the first few obstacles. This highlights the importance of taking pore-scale approach in the dynamical problems that involve heat convection in porous media.

Nomenclature

List of symbols

a	amplitude $= (max.\ sin\ (2\pi \cdot f \cdot t) - \ min\ .\ sin\ (2\pi \cdot f \cdot t))/2$
c_p	specific heat capacity (J K^{-1} kg^{-1})
C	capacitance (F)
d	obstacle distance from inlet (m)
D	particle diameter (m)
f	frequency (Hz)
$\mathscr{F}$	Fourier transform
h_o	external heat loss coefficient (W m^{-2} K^{-1})
k	thermal conductivity (W K^{-1} m^{-1})
n	Euclidean distance of the normalized Nusselt number at each particle
Nu	Nusselt number (−)
o	Discrete Fourier transform single sided amplitude spectrum of the normalized Nusselt number at each particle
p	pressure (Pa)
Pe	Peclet number (−)
Pr	Prandtl number (−)
q''	heat flux (W m^{-2})
R	resistance (Ω)
Re	Reynolds number (−)
St	$(f \cdot D)/u$
t	time (s)
T	temperature (K)
u	flow velocity (m s^{-1})
X_C	capacitive reactance (Ω)

***Greek** symbols*

μ	dynamic viscosity (kg m^{-1} s^{-1})
ε	porosity
ρ	density (kg m^{-3})
ϕ	phase
ω	angular frequency (rad s^{-1})
δ	measure of non-linearity
ψ	temperature/velocity

* Corresponding author.
E-mail address: Nader.Karimi@glasgow.ac.uk (N. Karimi).

https://doi.org/10.1016/j.icheatmasstransfer.2020.104639

Subscripts

amb	ambient
delay	delay
c	cut-off
D	based on Darcy
f	fluid
i	obstacle number
in	inlet
L	based on particle diameter size
ramp	function of ramp
ref	reference
x, y, z	Cartesian coordinates

Superscript

-	mean

1. Introduction

The dynamic response of forced convection in porous media to imposed disturbances is of high practical significance. Many natural and manmade systems involve forced convection within porous media in which the inlet flows are time dependent. Examples include fuel cells [1,2], heat exchangers [3] Stirling engines and pulse tube cryo-coolers as well as human circulatory systems [4]. The most conventional way of characterising the response of any physical system to input temporal disturbances is by working out the frequency response or transfer function [5]. This provides a strong means of predicting the system response to any arbitrary temporal disturbance with minimal computational effort. In this approach the response of system to harmonic inputs are measured/computed for a range of frequencies. Through using Fourier transformation, any arbitrary intake can be deconstructed into a group of harmonics. Since transfer function provides the response of the system to each of those harmonics, the total response can be readily devised through superposition.

Although transfer functions are very helpful in predicting the dynamic response, they are limited to linear systems. For that reason, prediction of the response of a nonlinear system to input disturbances often involves full simulations, which can be highly demanding. Hence, it is essential to evaluate linearity of different systems and determine the applicability of transfer function approach to prediction of their dynamics. This is particularly the case for thermofluid systems as the strong nonlinearity of momentum transfer often tends to dominate the dynamics of these systems [6] [7]. Nonetheless, slowly moving fluid systems can be, sometimes, modelled as linear systems [8]. Given the major convenience that linear dynamics offer, it is crucial to figure out under which conditions a system can be approximated as linear. The current work aims to answer this question addressing forced convection within a porous structure for which the fluid flow is relatively slow and therefore the dynamics might remain nearly linear.

A large number of articles reported studies on forced convection in porous media [9] [10] [11] [12] [13]. The general area of macroscopic analysis of forced convection in porous media has already received substantial attention. Numerous examples of steady ([14] [15] [16] [17]), unsteady ([3] [18]), turbulent flow ([19] [20] [21] [22]) and local non-equilibrium ([23] [24] [25] [26]) studies can be readily found in the literature. It is, however, known that macroscopic approach to heat convection in porous media is an approximative method and that a pore-scale understanding of the underlying physics is an important necessity. This is particularly the case for unsteady processes as they are more prone to being smeared out in the averaging exercises leading to macroscopic formulations [8,27]. Here, a brief review of the literature on the pore-scale analyses of forced convection of heat is put forward. The studies have been arranged in a chronological order to better represent the historical evolution of this branch of research on convection in porous media.

Fujii et al. [28] numerically investigated heat transfer in a two-dimensional model. Incorporating a steady laminar flow, they modelled a square bank consisting of five cylindrical obstacles with an in-line arrangement and solved Navier Stokes and energy equations. Isothermal boundary conditions were imposed on the tube wall and Reynolds number, Re_L, was varied between 60 and 300. Fujii et al. [28] discovered a connection between flow and heat transfer and the type of flow obstacles in the porous configuration. *Ma* and Ruth [29] conducted a numerical analysis of high Forchheimer number flow in a two-dimensional porous model. Their problem consisted of an interconnected three unit-cell capillary configuration in which Navier Stokes equations were solved. *Ma* and Ruth [29] developed the macroscopic momentum equations by applying the volume averaging concept and calculated macroscopic parameters such as permeability and Forchheimer number. They altered the Reynolds number, Re_D, between 0.01 and 100, and argued that the macroscopic response of the system involves nonlinear flow when $Re_D \approx 10$.

Nakayama et al. [30] examined steady heat and fluid flow in a two-dimensional anisotropic configuration. These authors modelled an in-line arrangement of square obstacles to represent a microscopic porous system. The square obstacles were set to constant temperature; higher than that of the inlet temperature. Navier Stokes and energy equations were solved numerically for a single unit cell structure and laminar flow regime. The results procured were then subject to volume averaging to analyse the macroscopic parameters similar to those of *Ma* and Ruth [29]. Nakayama et al. [30] compared the effects of increasing the Reynolds number with respect to the Nusselt number at two different modes of anisotropy. They concluded that when the system is modelled as isotropic, at 0° of anisotropy, there is very little augmentation in Nusselt number, *Nu*, as Reynolds number, *Re*, is increased. However, when the system has 45° anisotropy there is a sharp incline in *Nu* when $Re_L \geq 10$. More recently and inspired by Saito and Lemos [31] and Kuwahara et al. [32], Gamrat et al. [33] numerically studied heat transfer over square obstacles with low Reynolds number ranging between $0.05 \leq Re_D \leq 40$. Modelling the two-dimensional square obstacles in an in-line and staggered arrangement for a periodic unit cell, the flow was steady and laminar also, isothermal and isoflux boundary conditions were implemented. Gamrat et al. [33] found that, for a staggered arrangement, there is a greater change in Nusselt number by increasing Reynolds number compared with an inline arrangement. For both arrangements, higher porosities resulted in lower Nusselt numbers.

In a dynamic analysis, Kim and Ghiaasiaan [34] considered square particles in an inline arrangement with six unit cells simulating unsteady laminar flow, modulated by the external flow pulsations. The oscillatory flow had a frequency range of $20\ \text{Hz} \leq f \leq 64\ \text{Hz}$. Navier Stokes equations were solved using the commercial software FLUENT followed by the application of the volume averaging concept to calculate the macroscopic parameters for each unit cell. Kim and Ghiaasiaan [34] showed that the value of the cycle-averaged permeability coefficients were similar between steady and unsteady flows. However, the cycle-averaged Forchheimer coefficients were reported to be quite responsive to flow pulsation. As a result, the values recorded for steady flow were naturally greater. Variable parameters such as ε and Re_D were found to be the core cause of phase change between the velocity and pressure oscillations.

A two-dimensional laminar model containing square obstacles in an inline arrangement was analysed by Alshare et al. [35]. The Representative Elementary Volume (REV) was designated as a unit cell, subject to steady and unsteady flows in both isotropic and anisotropic conditions. The square obstacles were set to constant heat generating thermal boundary conditions. The flow angle was varied between 0° and 90° and *Re* was altered between 1 and 1000. For steady flows, the results were similar to those of Nakayama et al. [30] where the increase of Reynolds number led to a gradual increase of Nusselt number under

isotropic conditions. Additionally, for anisotropic conditions there was a drastic increase in Nusselt number with Reynolds number. Alshare et al. [35] further showed that the isotropic model was unaffected by the flow angle. However, permeability of the anisotropic model changed between the two principal permeabilities. Subsequently, Pathak and Ghiaasian [36] studied the effects of thermal dispersion and convective heat transfer in a laminar oscillating flow. Pathak and Ghiaasian [36] argued that a single unit cell model neglects the entrance effects complications and the phase lag, making the periodic boundary conditions unsuitable for oscillatory flows. As a result, they modelled an inline arrangement of two-dimensional square particles [36]. The oscillatory flow frequency was set between 0 and 100 Hz and the Reynolds number varied between 70 and 980. It was found that as the frequency increases there is an augmentation in the average convection coefficient and, for a higher Reynolds number a large average convection coefficient was reported. However, the average Nusselt number dropped at higher porosities.

Penha et al. [37] proposed a computational method to solve conjugate heat transfer with isothermal conditions for a three-dimensional porous medium including periodic REVs. The system was arranged in an aligned and staggered way; similar to that of Nakayama et al. [30] [38] and Kuwahara et al. [32]. A pair of pore-scale energy equations were solved for fluid and solid regions to characterise the conjugate heat transfer. This further allowed Penha et al. [37] to average the heat transfer coefficient as the temperature of the solid altered gradually, with respect to time-scale of the developing fluid. In a study of fuel cells, Yuan and Sundén [1] analysed heat transfer in a porous medium with the use of pore-scale energy eqs. A simplified two-dimensional porous model was developed within a parallel plate; with the top wall subject to a constant heat flux and the lower wall set to adiabatic conditions. This included a set of 5×5 cylindrical solid particles in an inline arrangement subject to a uniform flow. Yuan and Sundén [1] altered the operating conditions to simulate various scenarios and showed that Knudsen number was minuscule to overlook the rarefaction effect.

In a different work, Pathak et al. [39] studied conjugate heat transfer like that of Penha et al. [37] but with exposure to a laminar pulsating flow. This involved simulation of a two-dimensional system with seven aligned square rods which were considered as the REV and, pulsating frequency was altered between 0 and 60 Hz (at two different amplitudes). The pore-scale results were then used to work out the volume-averaged Darcy permeability, Nusselt number and Forchheimer coefficient showing that these parameters were highly responsive to pulsating flow and change in amplitude. Amongst other findings, Pathak et al. [39] stated that extrapolative approaches and relationships which are built on uniform consistent flow are not suitable for investigating periodic flow systems. In a similar study, Mulcahey et al. [40] examined the effects of oscillatory flows upon heat transfer and drag in a two-dimensional array of square obstacles imitating a heat exchanger. Extending the model from Pathak et al. [39] to ten unit-cells as the REV, the square particles were set to a constant temperature of 300 K whilst the inlet temperature was 200 K. Mulcahey et al. [40] found the drag coefficient plummeted with higher porosities and Re_L but had little or no sensitivity to the changes in the oscillation frequency of the flow. The Nusselt number was reported to augment with the decrease in the period of the pulsating flow and with the increase in Re_L. It was concluded that oscillatory flows could enhance heat transfer in heat exchanger tube bundles.

In their numerical investigation, Imani et al. [41] analysed the effects of ε, Re, Pr, thermal conductivity ratio and heat conduction on heat flux splitting at the boundary of a porous medium. They designed a channel with parallel plates, consisting of three different porous configurations of random, inline and staggered. The inlet was set to uniform velocity with the working fluid being air and water. The square obstacles were set to a constant heat flux and the parallel plates were assumed to be thermally insulated. The system was modelled under steady conditions with laminar flow ($1 \leq Re_L \leq 50$). Imani et al. [41] employed Lattice Boltzmann Method to solve for fluid flow and heat transfer and found that all the investigated parameters could influence heat flux splitting at the external boundary of the porous medium. However, the effects of some parameters were reliant on those of others such as the thermal conductivity ratio between solid and fluid.

Teruel [42] studied the entrance effects on heat transfer between the solid and fluid regions through porous media. They investigated a porous medium consisting of two-dimensional square obstacles in a staggered arrangement. The inlet temperature was set to be higher than the constant temperature at the fluid/solid interface. The system was modelled under microscopic laminar flow and periodic boundary conditions were applied to the outlet of the model. The volume averaging concept was utilised to obtain the interfacial heat transfer coefficient. The results showed that the flow was characterised by a developing region which could be multiple REVs in length showing agreement with Pathak and Ghiaasian [36]. Teruel concluded that the macroscopic energy equation model might show large discrepancies if the entrance effect was to be neglected [42].

Pore-scale, turbulent heat convection in a three-dimensional channel filled with porous media at a T-junction was numerically analysed by Yang et al. [43]. The porous media was modelled as square rectangular obstacles in both inline and staggered arrangements and fully developed flows were passed through the T-junction. The results showed that Nusselt number for the inline arrangement was less than that of the staggered arrangement. However, it was found that with increasing the flow rate, inline arrangement featured a dramatic increase in Nusselt number while, little increase was recorded for a staggered arrangement. Most recently, Jafarizade et al. [44] analysed heat convection in a metal foam geometry with the use of micro-tomography. The aluminium foam was simulated through a three-dimensional unsteady model with a Re_L of 10–200. The authors [44] presented the laminar model in terms of a structural factor to calculate the heat transfer coefficient. They found that with the addition of this new parameter, the accuracy of Nusselt number correlation was affected for application through ranges of pore diameter and porosity. However, Jafarizade et al. [44] argued that the developed correlation could still decently represent convection coefficient of the porous metallic foams. In another recent work by the same group, Afshari et al. [45] numerically studied thermal dispersion in granular porous media using a pore-scale model. Microscopic governing equations were used to solve the steady laminar flow of granular porous media. A direct numerical simulation was then carried out to calculate the macroscopic thermal dispersion. The system under investigation was simulated as a three-dimensional configuration with circular grains and varying diameters. Afshari et al. [45] discovered that when under advection dominated regime, normalized longitudinal dispersion coefficient increased with increases in the fluid to solid thermal conductivity ratio [46].

Ahmed et al. [47] investigated the thermal performance of a pipe partially filled with metal foams. A grooved metal foam was used to observe heat transfer and fluid flow characteristics. It was reported that the aspect ratio of 0.55 results in the optimal Nusselt number. Chakkingal et al. [48] studied the combined effects of natural and forced convection in a heated cavity filled with porous media. Richardson number was altered between 0.025 and 500 and it was found that heat transfer improves when forced convection is travelling in the same direction as natural convection. The reverse behaviour was noted for opposing forced and natural convection. Qin et al. [49] analysed the effects of flow boiling in a two-dimensional open-cell metal foam using Lattice Boltzmann method. The pore-scale study systematically varied Reynolds number, porosity and Rayleigh number, and showed that convective heat transfer is suppressed due to the bubble motion confinement within the metal foam.

It follows from the review of literature that, except for a few studies ([34] [35] [36] [39] [40]), the response of forced convection within

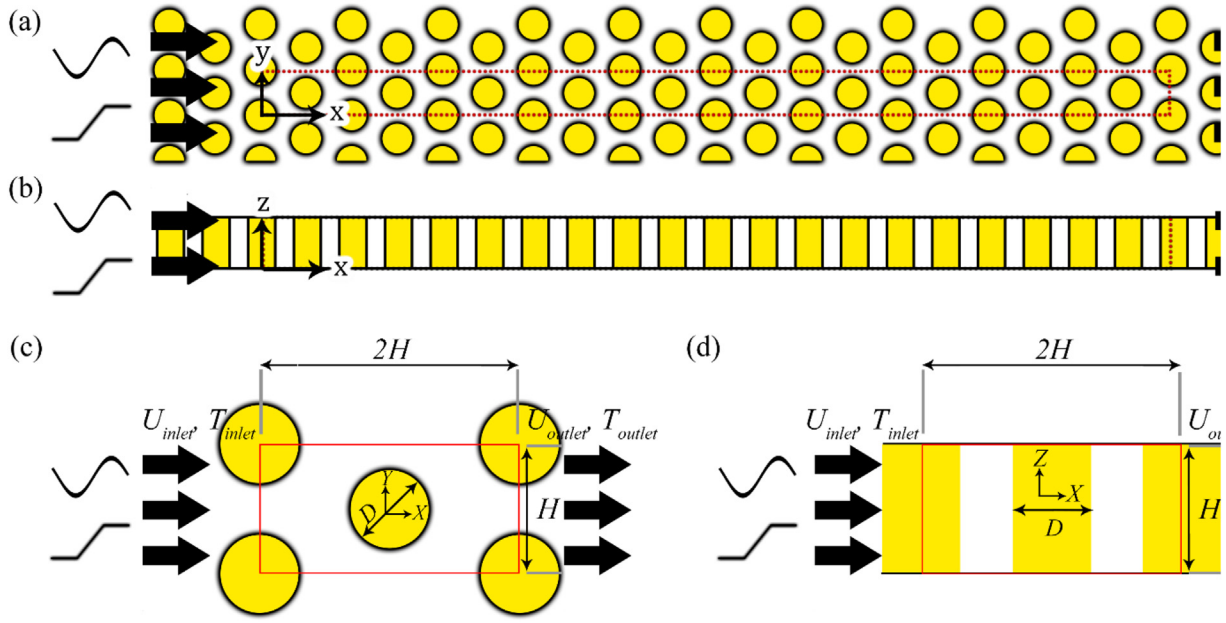

Fig. 1. A view of the terrain model used for unsteady investigations (a) x-y coordinate system (b) x-z coordinate system (c)computational unit for a single pore in x-y plane (d) computational unit for a single pore in x-z plane.

porous media to oscillating flows at the inlet has not been investigated at pore-scale. Further, the existing studies are mostly attentive to the value of Nusselt number and the factors influencing that under oscillating flow conditions. Consequently, the dynamics of heat transfer have comparatively received much less attention. As a result, our understanding of the dynamic response of porous media to incoming flow disturbances is still largely incomplete. The current study aims to address this issue.

2. Methodology

2.1. Problem configuration, governing equations and assumptions

A visual representation of the analysed pore-scale configuration is depicted in Fig. 1. This includes a three-dimensional model consisting of cylindrical obstacles in staggered arrangement in which a steady or temporally modulated flow enters from left-hand side. This configuration is subject to periodic boundary conditions on the upper and lower boundaries. The reason for the selection of such configuration will be discussed later.

Assuming a laminar flow, for the low Reynolds number considered in this study, the governing equations are as follows. The unsteady equations for the continuity of mass, momentum and energy are obtained from Ref. [50] and are expressed, respectively, as shown below.

$$\frac{\partial \rho}{\partial t} + \frac{\partial(\rho u_x)}{\partial x} + \frac{\partial(\rho u_y)}{\partial y} + \frac{\partial(\rho u_z)}{\partial z} = 0, \tag{1}$$

$$\rho\left(\frac{\partial u_x}{\partial t} + u_x\frac{\partial u_x}{\partial x} + u_y\frac{\partial u_x}{\partial y} + u_z\frac{\partial u_x}{\partial z}\right) = -\frac{\partial p}{\partial x} - \frac{\partial}{\partial x}\left[-2\mu\frac{\partial u_x}{\partial x} + \frac{2}{3}\mu\left(\frac{\partial u_x}{\partial x} + \frac{\partial u_y}{\partial y} + \frac{\partial u_z}{\partial z}\right)\right] - \frac{\partial}{\partial y}\left[-\mu\left(\frac{\partial u_x}{\partial y} + \frac{\partial u_y}{\partial x}\right)\right] - \frac{\partial}{\partial z}\left[-\mu\left(\frac{\partial u_z}{\partial x} + \frac{\partial u_x}{\partial z}\right)\right], \tag{2a}$$

$$\rho\left(\frac{\partial u_y}{\partial t} + u_x\frac{\partial u_y}{\partial x} + u_y\frac{\partial u_y}{\partial y} + u_z\frac{\partial u_y}{\partial z}\right) = -\frac{\partial p}{\partial y} - \frac{\partial}{\partial x}\left[-\mu\left(\frac{\partial u_x}{\partial y} + \frac{\partial u_y}{\partial x}\right)\right] - \frac{\partial}{\partial y}\left[-2\mu\frac{\partial u_y}{\partial y} + \frac{2}{3}\mu\left(\frac{\partial u_x}{\partial x} + \frac{\partial u_y}{\partial y} + \frac{\partial u_z}{\partial z}\right)\right] - \frac{\partial}{\partial z}\left[-\mu\left(\frac{\partial u_y}{\partial z} + \frac{\partial u_z}{\partial y}\right)\right], \tag{2b}$$

$$\rho\left(\frac{\partial u_z}{\partial t} + u_x\frac{\partial u_z}{\partial x} + u_y\frac{\partial u_z}{\partial y} + u_z\frac{\partial u_z}{\partial z}\right) = -\frac{\partial p}{\partial z} - \frac{\partial}{\partial x}\left[-\mu\left(\frac{\partial u_x}{\partial z} + \frac{\partial u_z}{\partial x}\right)\right] - \frac{\partial}{\partial y}\left[-\mu\left(\frac{\partial u_y}{\partial z} + \frac{\partial u_z}{\partial y}\right)\right] - \frac{\partial}{\partial z}\left[-2\mu\frac{\partial u_z}{\partial z} + \frac{2}{3}\mu\left(\frac{\partial u_x}{\partial x} + \frac{\partial u_y}{\partial y} + \frac{\partial u_z}{\partial z}\right)\right], \tag{2c}$$

$$\rho c_p\left(\frac{\partial T}{\partial t} + \frac{\partial u_x T}{\partial x} + \frac{\partial u_y T}{\partial y} + \frac{\partial u_z T}{\partial z}\right) = k_f\left(\frac{\partial^2 T}{\partial x^2} + \frac{\partial^2 T}{\partial y^2} + \frac{\partial^2 T}{\partial z^2}\right), \tag{3}$$

All parameters and variables have been reported in the nomenclature.

Furthermore, the porosity of the configuration could be controlled by adjusting the obstacle dimensions. In this case, circular obstacles with diameter of 0.05 m were fitted in the domain and porosity was varied by changing the axial and transversal distances of the obstacles. No-slip condition along with 300 K constant temperature were applied on all solid walls. The fluid properties were set to those of air or hydrogen under standard settings. The velocity of the fluid at the entrance was assumed to be constant and the temperature was 200 K. Also, the surface-averaged Nusselt number over the flow obstacles were monitored to evaluate the heat transfer amongst the fluid, as well as the solid region.

To find out the minimum number of the required flow obstacles, an initial set of simulations were performed whereby the entrance and exit were set to periodic boundary conditions, while other settings were unchanged. This would reproduce the unit element (see Fig. 1c) for the porous structure based on the approach presented by Saito and de Lemos [51]. It should be noted that although this model is the closest representation of an internal component inside a porous medium, it's

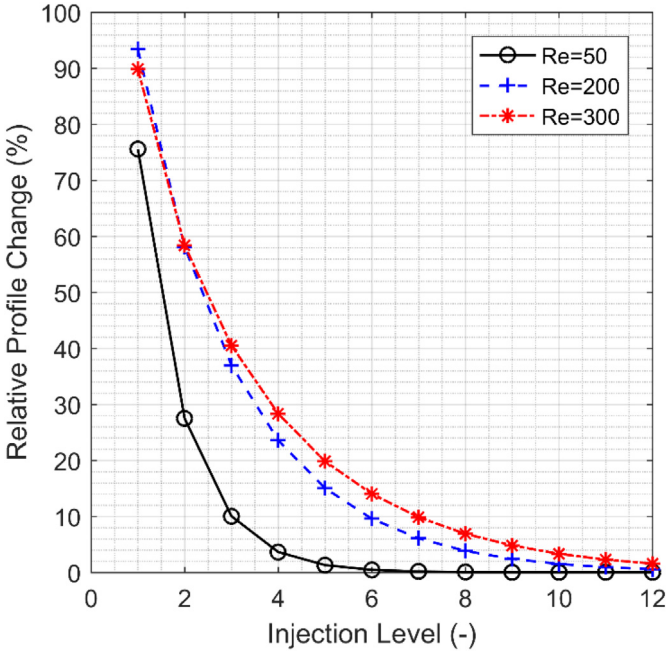

Fig. 2. Changes in the relative profile versus re-injection iterations for varying values of Reynolds numbers.

limited to a steady state environment. Therefore, a step-by-step methodology was developed to generate a representative model which could be used for unsteady simulations. The basic steady state unit model was used as a starting point, with velocity inlet and pressure outlet boundaries. A script was developed whereby the velocity and temperature profiles were re-injected from the exit to the entrance of the model. The simulations were re-run till the difference amid the entrance and exit profiles falls under a certain limit, denoted by Relative Profile Change (RPC):

$$RPC = \left(\sum_{profile} \frac{|\psi_{outlet} - \psi_{inlet}|}{\psi_{outlet}} \right) \bullet 100, \tag{4}$$

in which ψ is either temperature or velocity, and the RPC is summed over every point on the boundary as a percentage value. The results of the investigation for the selected Reynolds numbers have been summarised in Fig. 2. It could be seen that the profiles drop under 5% after 9 iterations have surpassed for the investigated Reynolds numbers. Beyond this point, the profiles effectively remain the same. Therefore, it was concluded that the representative model could be generated using a terrain made up of ten identical flow obstacles as shown in Fig. 1. To ensure the validity of this, the terrain geometry was tested at the same conditions as the periodic model. Investigations showed that the temperature and pressure profiles at the outlet almost exactly match those profiles after nine levels of injection. Furthermore, the results were very close to the profiles obtained using periodic boundary conditions confirming the proper build-up of the new model. The rest of the investigations reported in this study were performed on the model shown in Fig. 1a.

The inlet flow was modulated by varying the frequency and amplitude of the sinusoidal wave employed on the inlet velocity. That is:

$$u(0,t) = u_L \bullet (1 + asin(2\pi \bullet f \bullet t)). \tag{5}$$

It is well-known that any arbitrary temporal disturbance can be decomposed into a series of sine waves through application of Fourier transform. As a result, sine waves are the building blocks of temporal disturbances of all kinds and, for that reason here they are used as the primary input disturbances.

The Reynolds number was defined by the following relation [52].

$$Re_L = \frac{u_L \rho D}{\mu}. \tag{6}$$

Inside the pore-scale numerical model, heat is transported by forced convection complying with the Newton's law of cooling. That is [50].

$$q_f^{'} = h_o (T_f - T_{ref}). \tag{7}$$

which is defined at the surface of the obstacle. In order to assess the thermal response of the model, the surface-mean, time-dependent Nusselt Number was determined over all individual obstacles of the terrain model. The numerical value of the Nusselt number was acquired by the use of Eq. 8, as shown below [33].

$$Nu_L = \frac{q_f^{'} D}{k_f (T_f - T_{ref})}. \tag{8}$$

Three various values of Reynolds number (50,150,250) and porosity (0.87, 0.8 and 0.72) and six different frequencies between 0 and 2 Hz were investigated along with an inlet velocity disturbance with an amplitude of 30% of its steady value. Simulations were repeated for fluids of air, carbon dioxide and hydrogen, resulting in the total number of 162 unsteady simulations. The choice of the low frequencies is due to the low fluid velocity in the system which slows down the heat convection response. Thus, only long period (low frequency) flow disturbances are of interest.

2.2. Numerical methods

2.2.1. Computational techniques

A three-dimensional numerical model was developed in STAR-CCM + V12.04, which is a finite volume based Computational Fluid Dynamics (CFD) software. An adequately refined mesh of polyhedral cells was generated in the bulk region. Further, a number of tetrahedral or the so called “prism layer” cells were implemented near all solid surfaces with large gradients of flow properties (see Fig. 3). A second order discretization technique was employed to every equation along with a coupled solver which was adopted for achieving higher stability. For the unsteady simulations, the converged solution from similar steady state simulation was used as the initial condition. The foundation time-step was selected so that it was a factor of 100 below than that of the physical timescale. An improved time step was adopted for non-steady simulations for achieving higher accuracy. The steady state investigations were simulated until the residuals count fell under 10^{-6} for every equation. Furthermore, a very high value was selected for the maximum time-step number in unsteady cases, and the mean temperature at the exit of the model was monitored to check the convergence in time. The stoppage criterion was to terminate the simulations if the deviation in the last 1000 time-steps was under 0.5 K.

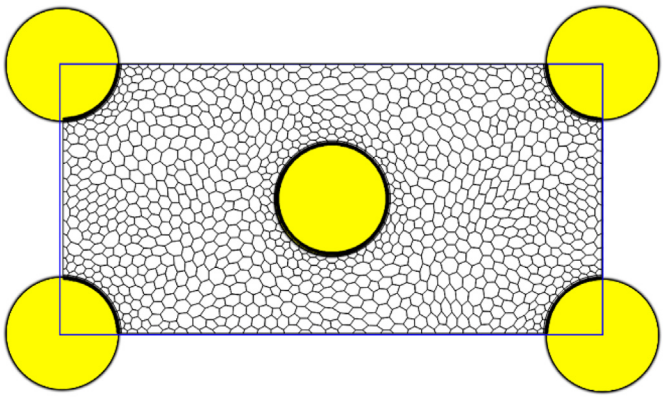

Fig. 3. Polyhedral staggered mesh with prism layers of a single pore.

Table 1
Comparison between Nusselt Number.

Re_D	*Nu* (simulated)	*Nu* (Kuwahara et al. [32])	*Nu* (Chen and Wung [53].)
50	3.71	4.71	4.06
100	5.43	5.92	5.54
150	6.65	6.89	6.65
200	7.61	7.80	7.58

2.2.2. Grid independency and validation

Nusselt numbers were calculated separately on each circular obstacle. These values were a single quantity for steady state simulations and a temporal variations plot was generated for unsteady cases. Temporal variations in the flow velocity were introduced at the inlet. The system response was represented by the temporal variations of Nusselt number over the obstacles. A series of successive refinements were undertaken on the computational mesh resulting in grids of roughly 2600, 45,000, 225,000, 377,000, 445,000, 613,000 and 2,570,000 cells, respectively. Examination of a single Reynolds number indicated that Nusselt number varied slightly with changing the grid in the range of 225,000–2,570,000 cells. Further refinement in the grid size did not show any noticeable change in the results. In fact, the changes in Nusselt number were minor even in the 225,000–613,000 cell range, and therefore a grid including 613,000 cells was used in this study.

To validate the numerical results, the calculated Nusselt numbers under steady state condition were compared with the empirical correlations of Chen and Wung [53] and Kuwahara et al. [32] developed for heat transfer in structures similar to that of the current study (see Table 1). These correlations are expressed by

$$\overline{Nu} = 0.78 Re^{0.45} Pr^{0.38}, \tag{9}$$

$$Nu = \left(1 + \frac{4(1+\varepsilon)}{\varepsilon}\right) + \frac{1}{2}(1+\varepsilon)^{1/2} Re^{0.6} Pr^{1/3}. \tag{10}$$

The former has been derived for staggered arrangement of pores while the latter was essentially extracted for square obstacles. Both correlations are valid in a wide range of Reynolds numbers and porosities. The settings are quite similar to the simulations discussed in Section 2.1.

For further validation, the results of an unsteady simulation using an in-house direct numerical simulation (DNS) code [54] were compared against the predictions made by the current simulations. The investigated geometry was a channel of 0.02 m $\times$0.002 m in dimensions. The air flow was laminar (Re = 150) and wall temperatures were maintained at 300 K. A 30% ramp-up variable temperature was applied at the inlet, and the temperature at three locations, namely x=0.0, 0.01, and 0.02 m were monitored. Fig. 4 shows a comparison between the two data-sets, featuring an excellent agreement. Although not shown here, comparison of the velocity profiles across the channel resulted in the same level of agreement. Therefore, it is concluded that the developed unsteady numerical model could predict the flow and heat transfer processes with adequate accuracy and resolution.

3. Results and discussion

The system shown in Fig. 1a, consisting of ten flow obstacles, can be considered as ten single-input single output (SISO) sub-systems [5]. In each of these, the velocity modulation at the far left of the figure is considered as the input and the resultant oscillations of the surface-averaged Nusselt number over each flow obstacle is the output. The spatio-temporal response of the porous configuration to a sinusoidal perturbation of the inlet flow velocity has been shown in Fig. 5. This figure includes snapshots of the flow field in four equally spaced points during one flow modulation cycle over a period of four seconds. The flow disturbance is advected by the mean flow and influences the flow

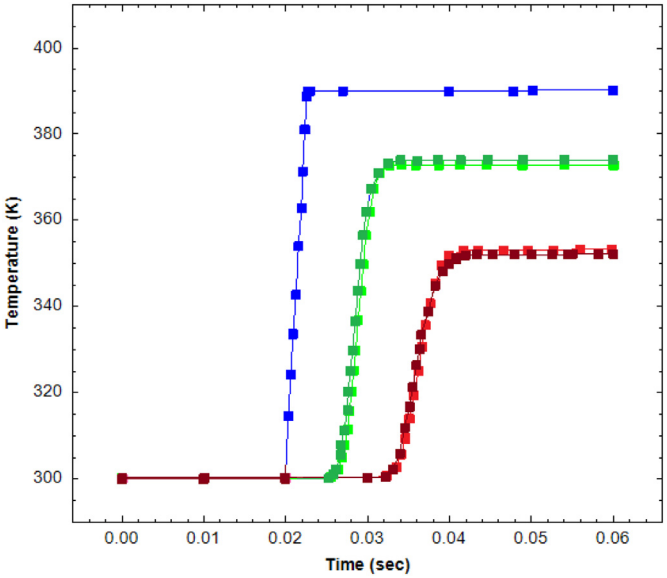

Fig. 4. Time trace of flow temperature at the inlet (blue), centre (green) and outlet (red), dark and light colour lines show the results of DNS and present simulations, respectively. (For interpretation of the references to colour in this figure legend, the reader is referred to the web version of this article.)

field around and behind the obstacles. The effects are strong for those obstacles that are positioned close to the flow inlet. Nonetheless, they decay as the disturbance further penetrates the porous system and the viscous effects annihilate the imposed velocity perturbation. An increased Re in Fig. 5a is reflected as the oscillation travels further downstream when compared to Fig. 5b. Temporal modification of the flow velocity around the obstacles perturbs the heat convection coefficient and leads to the oscillation of Nusselt number. These oscillations are expected to be more pronounced for the obstacles closer to the inlet and decrease in amplitude as the outlet is approached. This can be confirmed by visual inspection as a second oscillation (towards the outlet) within each system is recorded at a lower velocity. The analyses presented in this section aim to evaluate the linearity of the relation between the fluctuations in Nusselt number on different flow obstacles and those of the inlet flow.

Figs. 6a and 6b show a typical time trace of the flow velocity, along the centreline, as well as that of the surface-averaged Nusselt number over the first flow obstacle. Fig. 6b displays an obvious lag when the oscillation is compared with the flow velocity. The spectra of these traces are depicted in Figs. 6c and 6d, demonstrating that the frequency content of the system output (surface-averaged Nusselt number) is almost identical to that of the input (flow velocity oscillations). This is a clear indication of a linear system to which the classical theory of system dynamics could be applied [55]. However, Fig. 7 indicates that this is not always the case. This figure shows the spectrum of the Nusselt number fluctuations under three different conditions specified in the figure caption. In this figure, frequency has been non-dimensionalised through introducing a Strouhal number defined as $St = (f \cdot D)/u$. Clearly, the frequency response can include other harmonics different to that of the input. That is to say that although the flow velocity input contains only one frequency, the Nusselt number response involves two, or more, frequencies and hence it is nonlinear [6]. The same conclusion can be made through analysis of the phase portrait of Nusselt number and flow velocity traces at a selected frequency and over three different obstacles (see Fig. 8). The right column of Fig. 8 shows the cases for which the response remains nearly linear as the portraits are nearly axisymmetric. However, asymmetry of the phase portraits in the left column of this figure demonstrates a strong nonlinearity [56].

The spectral and phase portrait analyses shown in Figs. 6, 7 and 8

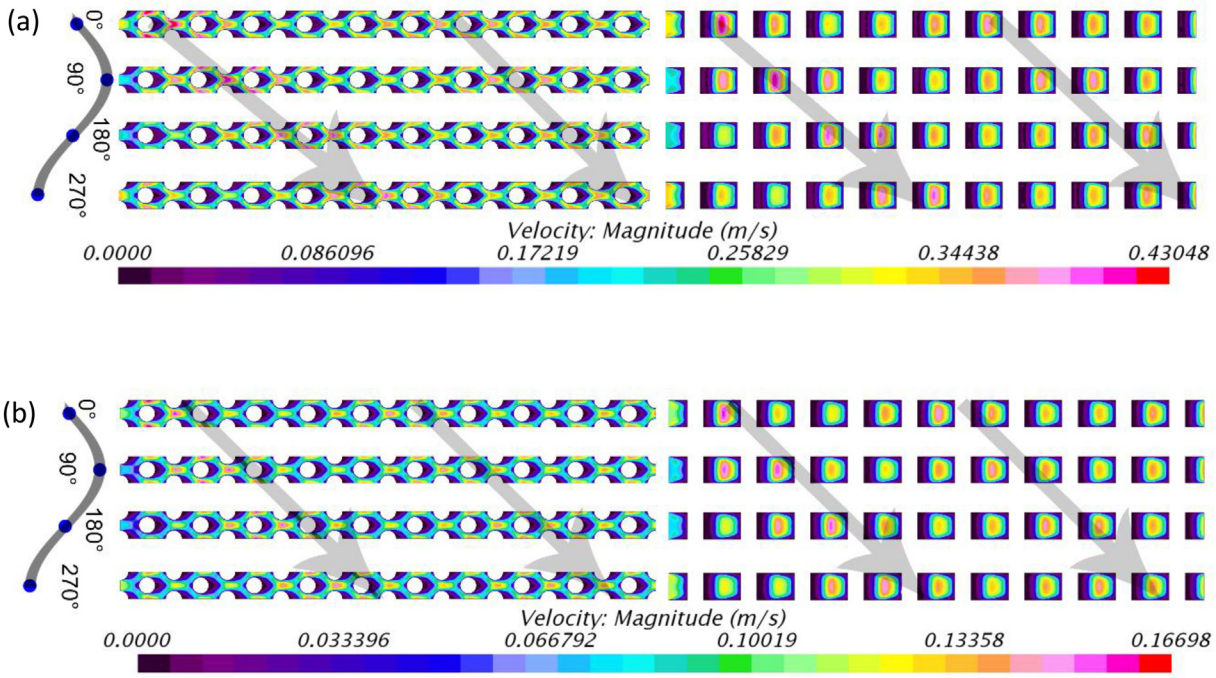

Fig. 5. Spatiotemporal evolution of the flow disturbance during advection throughout the system, left column: side view, right column: top view, (a) H_2, $\varepsilon = 0.804$ $Re = 150$ (b) H_2, $\varepsilon = 0.804$ $Re = 50$.

can detect nonlinear dynamics. However, they do not quantify the extent of nonlinearity. As shown in Fig. 7b, there could be situations in which the spectrum involves a relatively insignificant second peak. Yet, it is not obvious whether such cases can be still approximated as a linear response or not. It is therefore necessary to develop a rigorous quantitative measure of nonlinearity through which the linear and nonlinear responses of the system can be clearly distinguished. To resolve this issue, calculation of non-linearity was imported in order to assess alteration from a purely linear behaviour. The latter is conveyed through

$$\delta = \frac{n}{n - o} \tag{11}$$

in which δ is the extent of non-linearity, n, denotes Euclidean norm of the normalized Nusselt number logged over all obstacles and o is the discrete Fourier transform of that [57]. Here, the normalized Nusselt number is defined as $Normalised\ Nu = Nu_L \div \overline{Nu_L}$ where $\overline{Nu_L}$ is the surface-averaged Nusselt number over the obstacle under steady state condition. Eq. 11 assigns the value of zero to a truly linear system and sets one to an entirely nonlinear system. As a result, it always assigns a value between zero and one to any dynamical system [57]. A threshold can be then considered and the systems with the values of δ below that can be regarded as linear, while those with a measure of nonlinearity higher than the threshold are deemed nonlinear.

The numerical values of δ were evaluated for all obstacles and modulation frequencies and for all simulated configurations. For any given set of porosity or Reynolds number, the upper limit of δ (denoted by Max (δ)) was then found. Fig. 9 shows these maxima with changes in porosity and Reynolds number for the six inspected Strouhal numbers over each obstacle for CO_2. The figure caption also specifies the obstacle and Strouhal numbers where the upper limit was achieved. According to Fig. 9, changes in porosity and Reynolds number can majorly affect the upper limit of the degree of nonlinearity. For the lowest porosity, the maximum values of δ remains almost indifferent to Reynolds number. However, at higher values of porosity the maxima of δ can either increase or decrease by increases in Reynolds number. Fig. 9 shows that, in general, the variation of Max (δ) with porosity and Reynolds number is convoluted. It is, nonetheless, observed that regardless of porosity, for the lowest value of Reynolds number ($Re = 50$) the values of Max (δ) are the smallest in the figure and around 0.25. Physically, this can be explained by noting that nonlinearity in the current problem is dominated by the nonlinearity of momentum transfer (Eq. 2). Lowering the value of Reynolds number implies lower flow velocity which in turn weakens the nonlinearity of momentum transfer. This argument is qualitatively in keeping with the rationale behind Darcy and Darcy-Brinkmann models of flow in porous media which ignore the nonlinearity of momentum transfer [8]. However, unlike the general notion of macroscopic modelling, Fig. 9 shows that rises in Reynolds number do not inevitably result in stronger nonlinearity. Interestingly, the lowest value of Max (δ) in Fig. 9 is encountered at the highest Reynolds number.

Considering the value of $\delta = 0.25$ as the threshold of nonlinearity and sketching figures similar to Fig. 9 for other investigated fluids, the linear cases could be readily distinguished. For these, the classical theory of system dynamics and in particular the concept of transfer function can be developed to describe the response of thermal system to inlet flow modulations. Fig. 10 shows the transfer function of the thermal response for which the amplitude is defined as $|\mathscr{F}(Nu_i(St))|/|\mathscr{F}(u_{inlet}(St))|$. In this relation, $\mathscr{F}(Nu_i(St))$ is the Fourier transform of the surface-averaged Nusselt number for obstacle i and $\mathscr{F}(V_{inlet}(St))$ is the Fourier transform of the flow velocity at the inlet.

Fig. 10 shows the amplitude and non-dimensional delay of the transfer functions calculated for four linear cases. The data have been presented for the first and tenth flow obstacles as well as the average data for all ten obstacles. As a general trend, the rapid reduction of the amplitude with frequency is completely evident. That is to say that the surface-averaged Nusselt numbers over all obstacles respond more strongly to low frequency modulations. This behaviour is often regarded as low pass filtering and stems from the fact that the small frequency modulations deliver a lengthier time for the process of heat transfer to take place. As the frequency increases, the available duration for heat transfer declines and at certain frequency the system becomes essentially irresponsive to modulation and the amplitude approaches zero. This behaviour has been already reported in other thermofluid systems [7] [58]. The low-pass filtering characteristic of the response

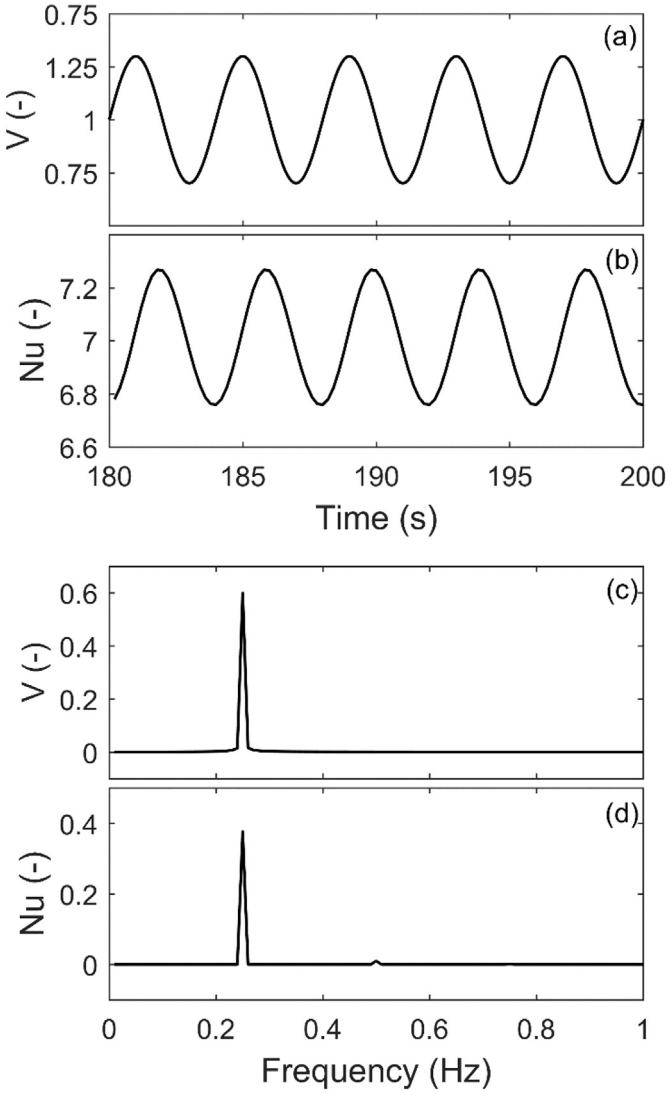

Fig. 6. (a) time trace of the inlet flow (b) time trace of the surface-averaged Nusselt number (c) spectrum of the inlet flow (d) spectrum of the surface-averaged Nusselt number for H_2, $\varepsilon = 0.804$ $Re = 50$.

allows for the development of an approximative formulation for the transfer function. A low pass filter allows passage of low frequency signals from 0 Hz to a cut-off frequency, f_c to pass and attenuates higher frequencies. This cut-off frequency can be found visually from the transfer function and following a procedure detailed in Refs. [59] [60], the general formulation for low pass filter is given by

$$Low\ pass\ filter = \vec{a} \bullet \frac{X_C}{\sqrt{R^2 + X_C^2}}, \tag{12a}$$

$$X_C = \frac{1}{2\pi fC}, \tag{12b}$$

whereby all terms are reported in the nomenclature. For the transfer functions shown in Fig. 10, this results in $A_{OUT} = A_{IN} \times \frac{\left(\frac{1}{2\pi fC}\right)}{\sqrt{1000^2 + \left(\frac{1}{2\pi fC}\right)^2}}$ in which A_{in} and A_{out} refer to the amplitude of the input (velocity) and output (Nusselt number). Fig. 10 shows that the developed low-pass filter closely approximates the average response across all ten obstacles and for the four investigated cases. Fig. 10 further shows that the amplitude of the response of the first obstacle grows in magnitude when the Re_L and of the structure increase. However, the frequency responses of the tenth obstacle are almost the same regardless of the values of Reynolds number and porosity. The strong dependency of the transfer function amplitude upon Reynolds number is to be expected as, in general, forced convection over a cylinder is significantly influenced by Reynolds number. Convergence of the responses over the tenth obstacle implies the existence of a global but negligibly low-amplitude response farther from the inlet.

Fig. 11 illustrates the outcomes of a statistical analysis conducted on all linear cases detected in this study (a total of 13 cases each consisting of 6 frequencies). To construct this figure, the amplitudes of the transfer function (as explained earlier) calculated for each obstacle were averaged over all investigated frequencies and the process was repeated for all detected linear cases. The arithmetic mean and standard deviation of the results are shown in Fig. 11. As expected, the first obstacle features the strongest average response and further shows the largest standard deviation amongst all obstacles. Moving towards the outlet of the system, the average amplitude drops quickly and so does the standard deviation of the amplitude. The rate of this drop is, however, non-uniform and the average amplitude decreases sharply over the first three obstacles. Yet, the amplitude decline slows down and after the fifth particle it becomes quite gradual. As a result, most of the amplitude dissipation occurs over the first three flow obstacles and the farther situated obstacles are of much less significance. This behaviour is an important result as it demonstrates that the problem under investigation is highly dependent upon pore-scale processes. Porous media macroscopic models of heat convection are often based on averaging over several pores with an inherent assumption that no sharp changes occur within those pores. Nonetheless, the current results show

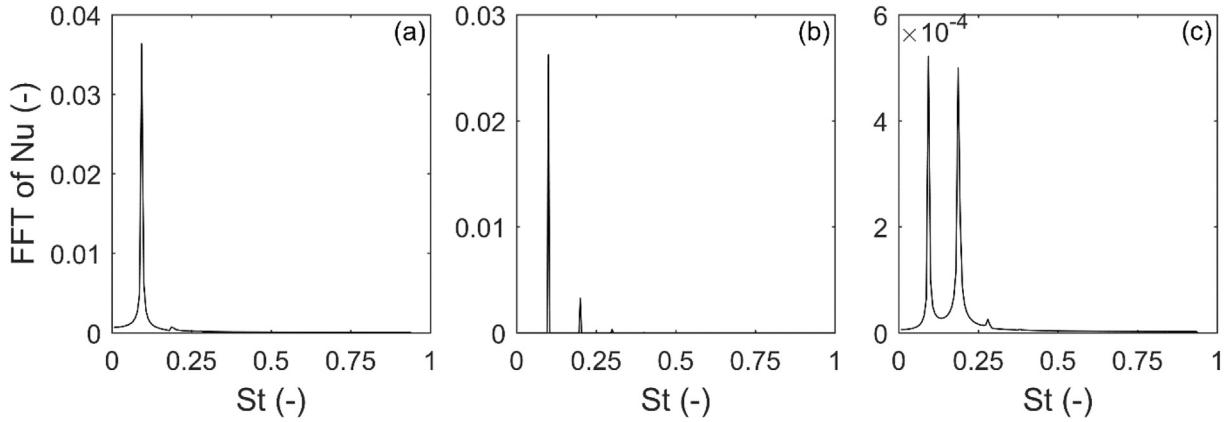

Fig. 7. Frequency content (spectrum) of Nusselt number oscillations (a) CO_2, $\varepsilon = 0.874$ $Re = 50$ $f = 0.25$ Hz, (b) Air, $\varepsilon = 0.874$ $Re = 150$ $f = 0.25$ Hz, (c) CO_2, $\varepsilon = 0.804$ $Re = 150$ $f = 0.25$ Hz.

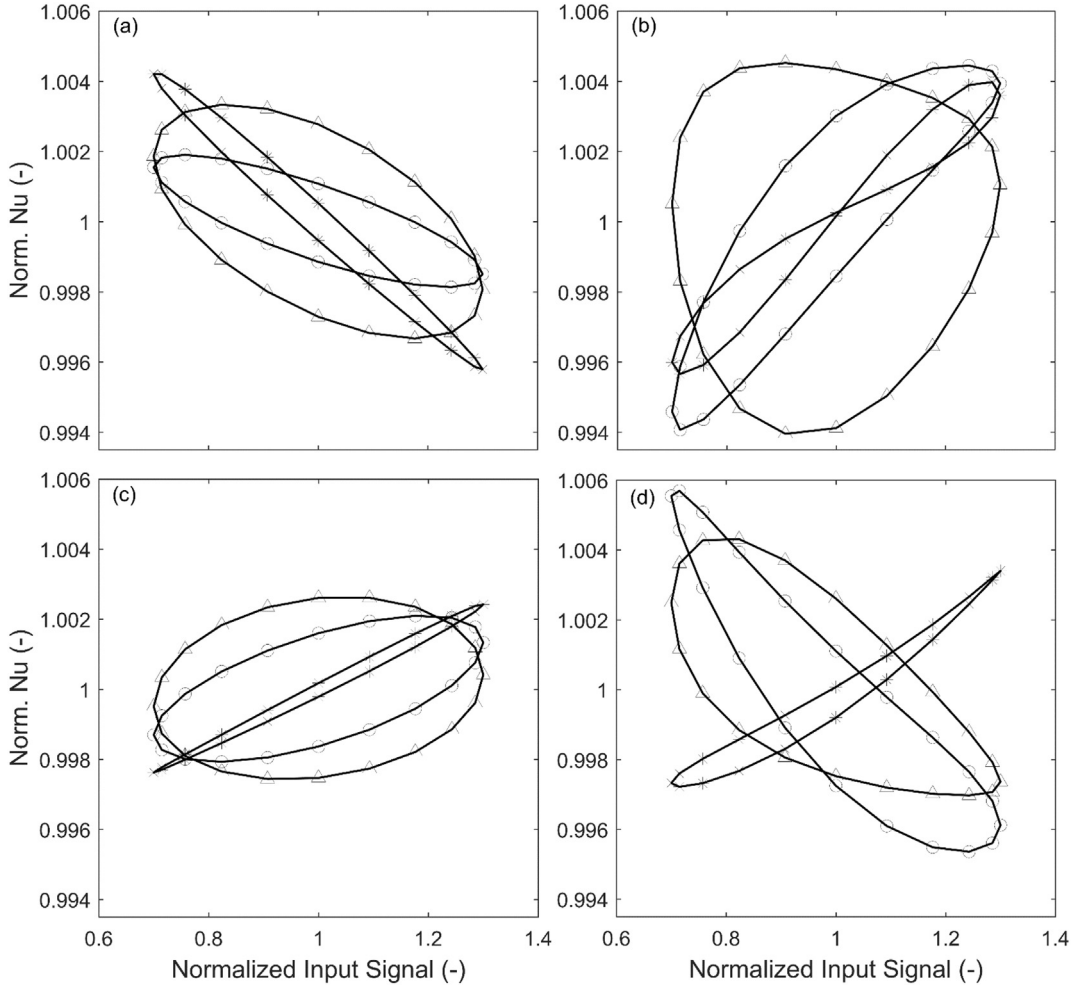

Fig. 8. Phase portrait of Nusselt number oscillations at $f = 0.25$ Hz, plus: first obstacle, circle: fifth obstacle, diamond: tenth obstacle. (a, c) H_2, $\varepsilon = 0.804$ $Re = 50$ & Air, $\varepsilon = 0.717$ $Re = 50$ -Linear dynamics (b, d) CO_2, $\varepsilon = 0.804$ $Re = 150$ & H_2, $\varepsilon = 0.804$ $Re = 150$-Nonlinear dynamics.

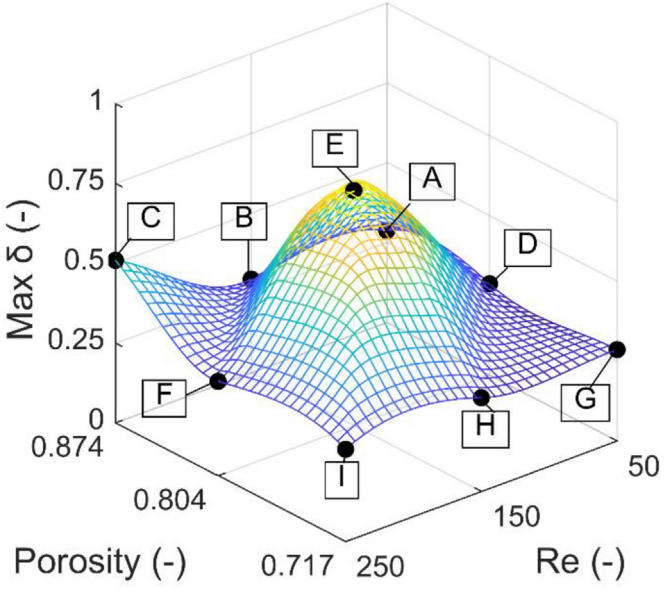

Fig. 9. The maximum values of the measure of nonlinearity for CO_2 simulations changing with porosity and Reynolds number A) $St = 1$, C2 B) $St = 0.375$, C3 C) $St = 0.125$, C2 D) $St = 0.375$, C5 E) $St = 0.125$, C8 F) $St = 0.375$, C3 G) $St = 0.375$, C5 H) $St = 0.125$, C6 I) $St = 0.375$, C7. C_i denotes flow obstacle i.

that response of the porous structure to flow modulations could vary strongly from one pore to another. Hence, adopting a pore-scale method appears to be an essential necessity in the problems that involve dynamic response of heat convection in porous media.

4. Conclusions

The dynamic response of forced convection in porous media to imposed oscillations on the inlet flow velocity was investigated through conduction of a pore-scale analysis. A porous-structure including several flow obstacles subject to constant wall temperature was exposed to harmonic oscillations of the flow velocity at the inlet. The dynamic relations between these oscillations and the resultant fluctuations in the surface-averaged Nusselt number over each obstacle were examined in detail. In particular, a novel measure of nonlinearity was introduced to quantify the nonlinearity of the Nusselt number response. The ultimate aim was to determine the transfer function of the porous medium so that the dynamic response of the medium to any arbitrary velocity disturbance could be figured out. Further, the limitations of transfer function were formally evaluated through measuring the linearity of the thermal response.

The crucial discoveries of this study can be summarised as below.

- Increases in pore-scale Reynolds number can push the dynamics towards nonlinearity. However, in contrast with a notion implied by the macroscopic models, further increases in Reynolds number may result in retrieving the linear response.

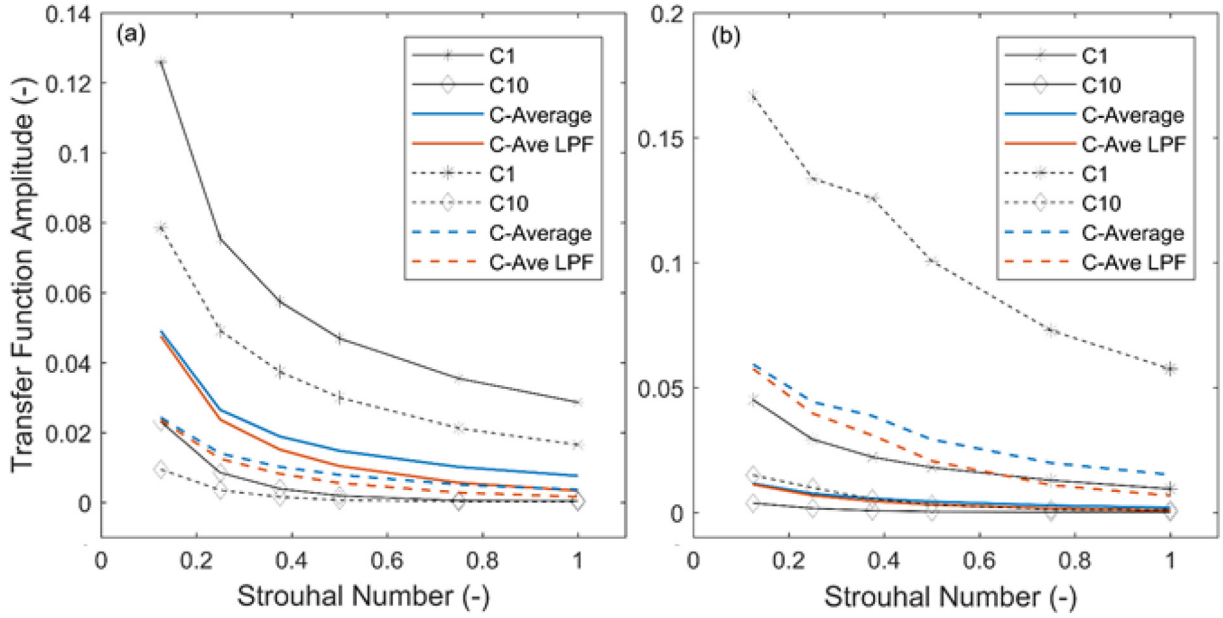

Fig. 10. Amplitude of transfer function (a) Fluid: Air, $\varepsilon = 0.874$ $Re = 50$ (solid line) & Air, $\varepsilon = 0.804$ $Re = 50$ (dashed line). (b) Air, $\varepsilon = 0.717$ $Re = 50$ (solid line) & Air, $\varepsilon = 0.717$ $Re = 250$ (dashed line). C_i denotes obstacle i.

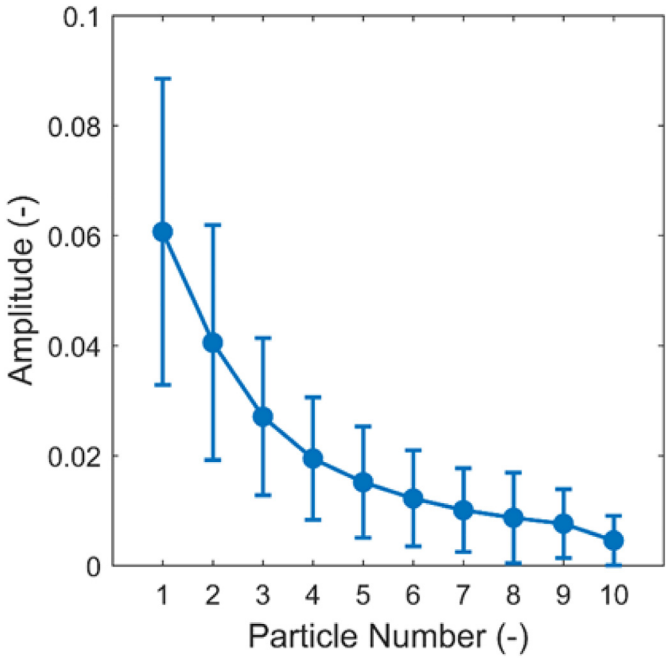

Fig. 11. Average and standard deviation of the amplitude of transfer function for all linear cases.

- The Nusselt number transfer functions developed for the linear cases, can be similar to a classical low-pass filter. This highlights the fact that the dynamics of heat convection are influenced most significantly by the low-frequency flow disturbances.
- The statistical analysis of the cases with linear dynamics showed that the thermal response of the porous structure is dominated by those of the first few obstacles. This clearly reflects the importance of utilising pore-scale modelling in the analysis of unsteady forced convection in porous media.

The future tasks include prediction of the dynamics of forced convection of heat in porous media under nonlinear conditions and complex fluids [61] [62].

Author statement

Rabeeah Habib: Analysis, writing.
Bijan Yadollahi: Analysis.
Nader Karimi: Supervision, fund acquiring, writing.
Mohammad Hossein Doranehgrad: Software.

Declaration of Competing Interest

The authors declare that they have no known competing financial interests or personal relationships that could have appeared to influence the work reported in this paper.

Acknowledgment

N. Karimi and B. Yadollahi acknowledge the financial support of Engineering and Physical Science Research Council through grant EP/N020472/1.

References

[1] J. Yuan, B. Sundén, On continuum models for heat transfer in micro/nano-scale porous structures relevant for fuel cells, Int. J. Heat Mass Transf. 58 (1–2) (2013) 441–456.
[2] Y. Wang, K.S. Chen, J. Mishler, S.C. Cho, X.C. Adroher, A review of polymer electrolyte membrane fuel cells: technology, applications, and needs on fundamental research, Appl. Energy 88 (2011) 981–1007.
[3] N. Targui, H. Kahalerras, Analysis of a double pipe heat exchanger performance by use of porous baffles and pulsating flow, Energy Convers. Manag. 76 (2013) 43–54.
[4] Y. Mahmoudi, K. Hooman, K. Vafai, Convective Heat Transfer in Porous Media, CRC Press, 2019.
[5] K. Ogata, System dynamics, Vol. 3 Prentice Hall, Upper Saddle River, NJ, 1998.
[6] A. Fattahi, S.M. Hosseinalipour, N. Karimi, On the dissipation and dispersion of entropy waves in heat transferring channel flows, Phys. Fluids 29 (8) (2017) 87104.
[7] A. Fattahi, S.M. Hosseinalipour, N. Karimi, Z. Saboohi, F. Ommi, On the response of a lean-premixed hydrogen combustor to acoustic and dissipative-dispersive entropy waves, Energy 180 (2019) 272–291.
[8] M. Kaviany, Principles of Heat Transfer in Porous Media, (1991).
[9] M.M. Bhatti, A. Zeeshan, R. Ellahi, O.A. Bég, A. Kadir, Effects of coagulation on the two-phase peristaltic pumping of magnetized prandtl biofluid through an endoscopic annular geometry containing a porous medium, Chin. J. Phys. 58 (2019) 222–234.
[10] R. Ellahi, S.M. Sait, N. Shehzad, Z. Ayaz, A hybrid investigation on numerical and analytical solutions of electro-magnetohydrodynamics flow of nanofluid through porous media with entropy generation, Int. J. Numer. Methods Heat Fluid Flow 30

(2) (2019) 834–854.
[11] S.Z. Alamri, R. Ellahi, N. Shehzad, A. Zeeshan, Convective radiative plane Poiseuille flow of nanofluid through porous medium with slip: an application of Stefan blowing, J. Mol. Liq. 273 (2019) 292–304.
[12] J. Prakash, D. Tripathi, A.K. Triwari, S.M. Sait, R. Ellahi, Peristaltic Pumping of Nanofluids through a Tapered Channel in a Porous Environment: Applications in Blood Flow, Symmetry (Basel) 11 (7) (2019) 868.
[13] R. Ellahi, S.M. Sait, N. Shehzad, N. Mobin, Numerical Simulation and Mathematical Modeling of Electro-Osmotic Couette–Poiseuille Flow of MHD Power-Law Nanofluid with Entropy Generation, Symmetry (Basel) 11 (8) (2019) 1038.
[14] Y. Mahmoudi, N. Karimi, Numerical investigation of heat transfer enhancement in a pipe partially filled with a porous material under local thermal non-equilibrium condition, Int. J. Heat Mass Transf. 68 (2014) 161–173.
[15] N. Karimi, D. Agbo, A. Talat Khan, P.L. Younger, On the effects of exothermicity and endothermicity upon the temperature fields in a partially-filled porous channel, Int. J. Therm. Sci. 96 (2015) 128–148.
[16] M. Torabi, N. Karimi, K. Zhang, Heat transfer and second law analyses of forced convection in a channel partially filled by porous media and featuring internal heat sources, Energy 93 (2015) 106–127.
[17] C. Dickson, M. Torabi, N. Karimi, First and second law analyses of nanofluid forced convection in a partially-filled porous channel – The effects of local thermal non-equilibrium and internal heat sources, Appl. Therm. Eng. 103 (2016) 459–480.
[18] P. Forooghi, M. Abkar, M. Saffar-Avval, Steady and unsteady heat transfer in a channel partially filled with porous media under thermal non-equilibrium condition, Transp. Porous Media 86 (1) (2011) 177–198.
[19] J. Yang, Q. Wang, M. Zeng, A. Nakayama, Computational study of forced convective heat transfer in structured packed beds with spherical or ellipsoidal particles, Chem. Eng. Sci. 65 (2) (2010) 726–738.
[20] M.B. Saito, M.J.S. de Lemos, A macroscopic two-energy equation model for turbulent flow and heat transfer in highly porous media, Int. J. Heat Mass Transf. 53 (11–12) (2010) 2424–2433.
[21] T. Lu, P.X. Jiang, Z.J. Guo, Y.W. Zhang, H. Li, Large-eddy simulations (LES) of temperature fluctuations in a mixing tee with/without a porous medium, Int. J. Heat Mass Transf. 53 (21–22) (2010) 4458–4466.
[22] N.F. Jouybari, M. Maerefat, M.E. Nimvari, A macroscopic turbulence model for reacting flow in porous media, Transp. Porous Media 106 (2) (2015) 355–381.
[23] D.G.P. Guthrie, M. Torabi, N. Karimi, Combined heat and mass transfer analyses in catalytic microreactors partially filled with porous material - the influences of nanofluid and different porous-fluid interface models, Int. J. Therm. Sci. 140 (2019) 96–113.
[24] G. Hunt, N. Karimi, B. Yadollahi, M. Torabi, The effects of exothermic catalytic reactions upon combined transport of heat and mass in porous microreactors, Int. J. Heat Mass Transf. 134 (2019) 1227–1249.
[25] A. Saeed, N. Karimi, G. Hunt, M. Torabi, On the influences of surface heat release and thermal radiation upon transport in catalytic porous microreactors—a novel porous-solid interface model, Chem. Eng. Process. Process Intensif. 143 (2019) 107602.
[26] G. Hunt, N. Karimi, M. Torabi, Two-dimensional analytical investigation of coupled heat and mass transfer and entropy generation in a porous, catalytic microreactor, Int. J. Heat Mass Transf. 119 (2018) 372–391.
[27] D.A. Nield, A. Bejan, *Convection in porous media*, 5th Editio, (2017).
[28] M. Fujii, T. Fujii, T. Nagata, A numerical analysis of laminar flow and heat transfer of air in an in-line tube bank, Numer. Heat Transf. 7 (1) (1984) 89–102.
[29] H. Ma, D.W. Ruth, The microscopic analysis of high forchheimer number flow in porous media, Transp. Porous Media 13 (2) (1993) 139–160.
[30] A. Nakayama, F. Kuwahara, T. Umemoto, T. Hayashi, Heat and fluid flow within an anisotropic porous medium, J. Heat Transf. 124 (4) (2002) 746–753.
[31] M.B. Saito, M.J.S. de Lemos, Interfacial heat transfer coefficient for non-equilibrium convective transport in porous media, Int. Commun. Heat Mass Transf. 32 (5) (2005) 666–676.
[32] F. Kuwahara, M. Shirota, A. Nakayama, A numerical study of interfacial convective heat transfer coefficient in two-energy equation model for convection in porous media, Int. J. Heat Mass Transf. 44 (6) (2001) 1153–1159.
[33] G. Gamrat, M. Favre-Marinet, S. Le Person, Numerical study of heat transfer over banks of rods in small Reynolds number cross-flow, Int. J. Heat Mass Transf. 51 (3–4) (2008) 853–864.
[34] S.-M. Kim, S.M. Ghiaasiaan, Numerical Modeling of Laminar Pulsating Flow in Porous Media, J. Fluids Eng. 131 (4) (2009) 1–9 041203.
[35] A.A. Alshare, P.J. Strykowski, T.W. Simon, Modeling of unsteady and steady fluid flow, heat transfer and dispersion in porous media using unit cell scale, Int. J. Heat Mass Transf. 53 (9–10) (2010) 2294–2310.
[36] M.G. Pathak, S.M. Ghiaasiaan, Convective heat transfer and thermal dispersion during laminar pulsating flow in porous media, Int. J. Therm. Sci. 50 (4) (2011) 440–448.
[37] D.J. Lopez Penha, S. Stolz, J.G.M. Kuerten, M. Nordlund, A.K. Kuczaj, B.J. Geurts, Fully-developed conjugate heat transfer in porous media with uniform heating, Int. J. Heat Fluid Flow 38 (2012) 94–106.
[38] A. Nakayama, F. Kuwahara, T. Hayashi, Numerical modelling for three-dimensional heat and fluid flow through a bank of cylinders in yaw, J. Fluid Mech. 498 (498) (2004) 139–159.
[39] M.G. Pathak, T.I. Mulcahey, S.M. Ghiaasiaan, Conjugate heat transfer during oscillatory laminar flow in porous media, Int. J. Heat Mass Transf. 66 (2013) 23–30.
[40] T.I. Mulcahey, M.G. Pathak, S.M. Ghiaasiaan, The effect of flow pulsation on drag and heat transfer in an array of heated square cylinders, Int. J. Therm. Sci. 64 (2013) 105–120.
[41] G. Imani, M. Maerefat, K. Hooman, Pore-scale numerical experiment on the effect of the pertinent parameters on heat flux splitting at the boundary of a porous medium, Transp. Porous Media 98 (3) (2013) 631–649.
[42] F.E. Teruel, Entrance effect on the interfacial heat transfer and the thermal dispersion in laminar flows through porous media, Int. J. Therm. Sci. 104 (2016) 172–185.
[43] G. Yang, B. Weigand, A. Terzis, K. Weishaupt, R. Helmig, Numerical simulation of turbulent flow and heat transfer in a three-Dimensional Channel coupled with flow through porous structures, Transp. Porous Media 122 (1) (2018) 145–167.
[44] A. Jafarizade, M. Panjepour, M. Meratian, M. Davazdah Emami, Numerical simulation of gas/solid heat transfer in metallic foams: a general correlation for different porosities and pore sizes, Transp. Porous Media 127 (2) (2019) 481–506.
[45] S. Afshari, S.H. Hejazi, A. Kantzas, Pore-level modeling of effective longitudinal thermal dispersion in non-isothermal flows through granular porous media, Chem. Eng. Sci. 199 (2019) 451–462.
[46] M. Mottaghi, S. Kuhn, Numerical investigation of well-structured porous media in a milli-scale tubular reactor, Chem. Eng. Sci. 208 (2019) 1–13 115146.
[47] H.E. Ahmed, O.T. Fadhil, W.A. Salih, Heat transfer and fluid flow characteristics of tubular channel partially filled with grooved metal foams, Int. Commun. Heat Mass Transf. 108 (2019) 104336.
[48] M. Chakkingal, J. de Geus, S. Kenjereš, I. Ataei-Dadavi, M.J. Tummers, C.R. Kleijn, Assisting and opposing mixed convection with conjugate heat transfer in a differentially heated cavity filled with coarse-grained porous media, Int. Commun. Heat Mass Transf. 111 (2020) 104457.
[49] J. Qin, Z.G. Xu, Z.Y. Liu, F. Lu, C.Y. Zhao, Pore-scale investigation on flow boiling heat transfer mechanisms in open-cell metal foam by LBM, Int. Commun. Heat Mass Transf. 110 (2020) 104418.
[50] Á.L. De Bortoli, G.S.L. Andreis, F.N. Pereira, Equations of fluid dynamics, Modeling and Simulation of Reactive Flows, 2015, pp. 35–51.
[51] M.B. Saito, M.J.S. de Lemos, A correlation for interfacial heat transfer coefficient for turbulent flow over an array of square rods, J. Heat Transf. 128 (5) (2006) 444.
[52] H.A. Stone, C. Duprat, Low-reynolds-number flows, Fluid-Structure Interactions in Low-Reynolds-Number Flows, 4 2016, pp. 25–77.
[53] C.J. Chen, T.-S. Wung, Finite analytic solution of convective heat transfer for tube arrays in Crossflow: part II—heat transfer analysis, J. Heat Transf. 111 (3) (1989) 641–648.
[54] L. Christodoulou, N. Karimi, A. Cammarano, M. Paul, S. Navarro-Martinez, State prediction of an entropy wave advecting through a turbulent channel flow, J. Fluid Mech. 882 (2020) A8.
[55] K. Ogata, Y. Yang, Modern Control Engineering, Vol 17 Pearson, NJ, Upper Saddle River, 2010.
[56] H.S. Strogatz, Nonlinear Dynamics and Chaos: With Applications to Physics, Biology, Chemistry, and Engineering, Second ed., CRC Press, 2015.
[57] W.H. Moase, M.J. Brear, C. Manzie, The forced response of choked nozzles and supersonic diffusers, J. Fluid Mech. 585 (2007) 281–304.
[58] N. Karimi, Response of a conical, laminar premixed flame to low amplitude acoustic forcing - A comparison between experiment and kinematic theories, Energy 78 (2014) 490–500.
[59] A. Banerjee, Automated Electronic Filter Design, Springer International Publishing, Cham, 2018.
[60] A. Izadian, Fundamentals of Modern Electric Circuit Analysis and Filter Synthesis, Springer International Publishing, Cham, 2019.
[61] O. Mahian, L. Kolsi, M. Amani, P. Estellé, G. Ahmadi, C. Kleinstreuer, J.S. Marshall, M. Siavashi, R.A. Taylor, H. Niazmand, S. Wongwises, T. Hayat, A. Kolanjiyil, A. Kasaeian, I. Pop, Recent advances in modeling and simulation of nanofluid flows-Part I: fundamentals and theory, Phys. Rep. 790 (2019) 1–48.
[62] O. Mahian, L. Kolsi, M. Amani, P. Estellé, G. Ahmadi, C. Kleinstreuer, J.S. Marshall, R.A. Taylor, E. Abu-Nada, S. Rashidi, H. Niazmand, S. Wongwises, T. Hayat, A. Kasaeian, I. Pop, Recent advances in modeling and simulation of nanofluid flows—Part II: applications, Phys. Rep. 791 (2019) 1–59.